Highlights

Outdoor Characterization of Photocurrent-Based Focal Tracking in a Tracking-Integrated Micro-Concentrator Photovoltaic System

Fernando Dávalos Hernández, Arturo Díaz-Ponce, Iván Trejo-Zúñiga, Rosa C. Anguiano Cota, Pedro M. Rodrigo, María A. Ceballos, Álvaro Valera-Albacete, Florencia Almonacid, Eduardo F. Fernández

- A 5,049-sample field record characterizes internal focal tracking
- Estimated aperture efficiency is 23.41% over 6.121 h of accepted support
- A post-tuning phase yields a 28.47% aperture estimate
- Solar-position context and late response losses define observed operation
- Fixed-silicon scenarios use equal aperture and explicitly stated assumptions

Outdoor Characterization of Photocurrent-Based Focal Tracking in a Tracking-Integrated Micro-Concentrator Photovoltaic System

Fernando Dávalos Hernández[a,*], Arturo Díaz-Ponce[b,c], Iván Trejo-Zúñiga[c], Rosa C. Anguiano Cota[d], Pedro M. Rodrigo[a], María A. Ceballos[e], Álvaro Valera-Albacete[e], Florencia Almonacid[e], Eduardo F. Fernández[e]

[a] *Universidad Panamericana, Facultad de Ingeniería, Jose María Escrivá de Balaguer 101, Villas Bonaterra, Aguascalientes, 20296, Aguascalientes, Mexico*
[b] *SECIHTI – Centro de Investigaciones en Óptica, A.C., Unidad Aguascalientes, Prol. Constitución 607, Fracc. Reserva Loma Bonita, Aguascalientes, 20200, Aguascalientes, Mexico*
[c] *Laboratory of Energy Innovation and Intelligent and Sustainable Agriculture (LEIISA), Universidad Tecnológica de San Juan del Río, Av La Palma No 125 Vista Hermosa, San Juan del Río, 76800, Querétaro, Mexico*
[d] *Facultad de Ingeniería, Universidad Autónoma de Baja California (UABC), Blvd. Benito Juárez SN, Mexicali, 21280, Baja California, Mexico*
[e] *Advances in Photovoltaic Technology (AdPVTech), CEACTEMA, University of Jaén, Las Lagunillas Campus, Jaén, 23071, Jaén, Spain*

Abstract

Tracking-integrated concentrator photovoltaics preserve fixed external optics while moving the receiver to follow the evolving focal region. Their field performance therefore depends on both optical collection and internal positioning, rather than on external solar pointing alone. This work characterizes a photocurrent-feedback controller and custom ESP32 acquisition system for a wide-acceptance-angle tracking-integrated micro-concentrator photovoltaic (WiT-CPV) prototype. The principal experiment is the 4 November 2026 outdoor record in Aguascalientes, Mexico: 5,049 observations between 09:52 and 16:05, with 6.121 h of accepted integration support and no ADC clipping. Sequential short-circuit-current and open-circuit-voltage measurements yield an estimated available maximum-power-point energy of 3.746 Wh for an assumed fill factor of 0.82. Relative to the 0.002497-m^2 lens aperture and the coplanar pyranometric irradiation of 6.408 kWh m^{-2}, the energy-weighted efficiency estimate is 23.41%. The command-delimited 12:32–13:53 post-tuning phase yields an aperture estimate of 28.47% without additional logged operator commands. Solar-position data contextualize the operating trajectory, while the complete record retains tuning interventions and late response degradation. Reference sensitivity is examined rather than treated as an independent tracking-accuracy measurement. An equal-aperture silicon comparison is reported as a conditional constant-efficiency scenario, not a simultaneous panel experiment. The results establish an aperture-referenced field characterization and identify the measurements needed to validate delivered power, net energy and angular tracking accuracy.

Keywords: Tracking-integrated CPV, Focal tracking, Photocurrent feedback, Aperture efficiency, Outdoor characterization, Silicon photovoltaic benchmark

*Corresponding author. Email: fdavalos@up.edu.mx

1. Introduction

Photovoltaic energy collection depends on the relationship between solar direction, collector orientation and device response. Conventional one- and two-axis trackers improve this relationship by moving the module or concentrator as a whole, at the cost of actuation, support and control requirements [1, 2, 3]. In concentrating photovoltaics (CPV), optical alignment is especially important because displacement of the focal distribution can reduce the fraction intercepted by a small receiver [4].

Tracking-integrated CPV transfers part or all of the required motion inside the module [5]. Microtracking lens arrays, internally translated receivers and hybrid diffuse-light collection illustrate different ways of decoupling focal alignment from large external motion [6, 7, 8]. This distinction matters when interpreting field performance: moving a receiver beneath fixed optics does not make the optical aperture normal to the Sun, nor does it eliminate the finite angular and mechanical operating range of the assembly.

The wide-acceptance-angle tracking-integrated micro-concentrator photovoltaic (WiT-CPV) prototype studied here was previously reported with its optical and mechanical design, azimuthal cell rotation and first-generation controller [9]. Its receiver follows the moving focal region of a biconvex aspheric lens along a mechanically constrained trajectory. Knowledge of solar position alone does not establish the corresponding receiver coordinates: optical geometry, mounting and kinematics must also be known. Photocurrent provides a useful local feedback signal, although irradiance, temperature and spectrum can change it independently of alignment.

The present contribution is a field characterization of this coupled system using the complete acquired record of 4 November 2026. It connects measured electrical signals and stage coordinates to an explicitly estimated aperture-level output, places the response in solar-position context, and discloses data gaps and operational interventions. A fixed-silicon scenario provides an area-normalized engineering reference without substituting a simulation for an unperformed experiment. This focus replaces comparisons between heterogeneous development sessions with a traceable principal case; it does not constitute a controlled comparison of controller versions or a validation of net energy production.

2. System and Control

2.1. Optical and mechanical architecture

The prototype combines fixed primary optics, a multi-junction photovoltaic receiver and a two-axis actuated stage. Guided mechanical motion follows the curved focal trajectory associated with the Petzval surface; the detailed optomechanical construction is described in [9]. The lens aperture used in the present analysis is $A_L = 0.002497\ \mathrm{m}^2$. Coordinates X and Y denote the project's azimuth and elevation axes, respectively. They are commanded step coordinates, not independently measured solar or receiver angles. The acquisition does not provide a calibrated steps-to-angle transformation or an independent measurement of focal-position error.

2.2. Controller and measurement chain

An ESP32-based controller provides wireless command/telemetry interfaces and commands two TMC2209 stepper drivers. A 24-bit ADS122C04 converter acquires the photocurrent, pyranometer and cell-voltage channels. The photocurrent chain uses a nominal 0.130-Ω shunt for

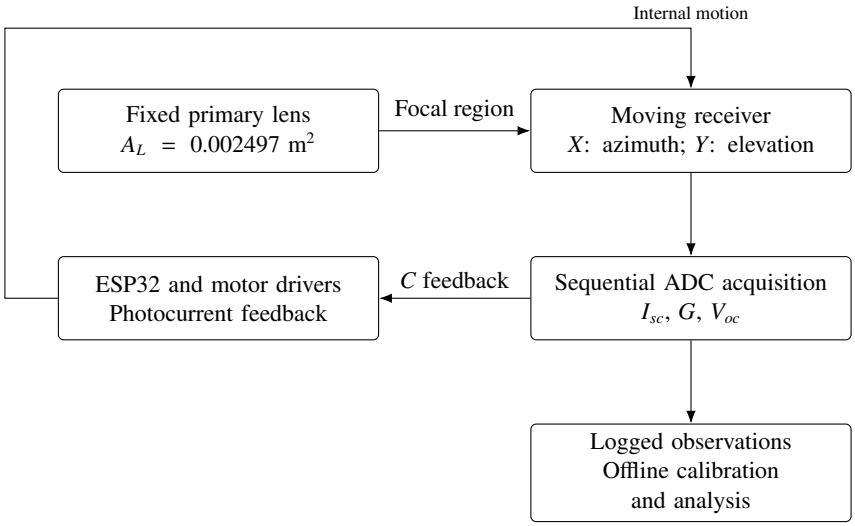


Figure 1: Functional architecture of the evaluated system. Only the receiver is repositioned; internal tracking does not reorient the external aperture. Electrical channels are acquired sequentially, and the offline power estimate is not feedback from a measured MPP load.

the evaluated PCB V2 configuration, an external gain of 20 and a 2.048-V reference. Open-circuit voltage is acquired through a factor-of-two divider, and an Apogee SP-212 provides the irradiance reference. The functional measurement and control paths are summarized in Fig. 1.

The cell is switched between short-circuit-current and open-circuit-voltage measurement states. Current, irradiance and voltage therefore represent sequential conversions rather than a simultaneous electrical operating point. The periodic `TEL` messages contain separate telemetry averages and fine-tuning counters; they are not interchangeable with the coordinate/ electrical observations used for the quantitative analysis.

2.3. Evaluated control and implementation provenance

The raw record identifies the deployed firmware as `1.1.3-ws`. The controller performs photocurrent-feedback fine tuning, with configurable step bounds, current-change thresholds, peak-proximity settings and axis-search cycles. Its log reports adaptive-step diagnostics and periodic reference resets. Pyranometer input supports illumination-related operating logic, but the offline I_{sc}/G ratio used below must not be interpreted as a verified samplewise feedback law of the evaluated firmware.

The available development source has subsequently changed; in particular, later revisions address current-change, near-peak and deadband behavior. Those later equations and features are not attributed to the recorded deployment. Accordingly, this article describes the evaluated controller at the level supported by version identifiers and logged behavior, rather than presenting unverified branch equations as an exact specification of its binary. The experiment includes parameter updates and manual positioning commands. It is an operational field characterization with disclosed tuning, not a fixed-parameter autonomous trial, an ablation study or proof that each protective control regime operates as intended.

3. Experimental and Analytical Methods

3.1. Site, acquisition and solar-position reference

The principal acquisition took place on 4 November 2026 in Aguascalientes, Mexico. The supplied SunCalc printout identifies latitude 21.87304° N and longitude 102.28282° W and tabulates solar azimuth and elevation at 15-min intervals [10]. The field conditions were described as clear by the experimenter; this is a field observation, not an independently measured classification of direct and diffuse irradiance. Brief irradiance anomalies are retained and examined.

Time plots use the local acquisition clock. The log has no encoded time-zone offset, so matching to the supplied local-time SunCalc table is an explicit clock-alignment assumption, not an independent timing calibration. Linear interpolation between the printed solar positions supplies context at observation times. It does not improve the ephemeris resolution or measure stage accuracy. Azimuth is measured clockwise from north and elevation above the horizon. Neither absolute solar azimuth nor its span equals the collector incidence angle. The acquisition package does not establish absolute external-optics tilt/azimuth, so conversion to a validated optical acceptance envelope is not attempted.

3.2. Offline calibration and data-quality rules

Let C, V and P denote the signed 24-bit photocurrent, voltage and pyranometer codes, with positive full scale $D = 8{,}388{,}607$. Offline conversion is

$$I_{sc} = \frac{2.048C}{20DR_s}, \qquad V_{oc} = \frac{2(2.048)V}{D}, \qquad G = \frac{2048P}{0.2D}, \quad R_s = 0.130\ \Omega. \tag{1}$$

The resulting units are A, V and W m^{-2}. The pyranometer sensitivity is 0.2 mV/(W m^{-2}); using 2.0 would understate irradiance tenfold. The raw channels are not exchanged: `C` is photocurrent and `P` is pyranometer output. The same physical shunt applies throughout this record; a software conversion update at the hub does not define a physical shunt change in the raw acquisition.

The experimenter confirms that the SP-212 was mounted in the same plane as the concentration lens. Thus G is measured global irradiance in the fixed lens-aperture plane, and GA_L estimates incident solar power on that aperture. No additional cosine projection is applied: the beam's geometric projection onto the receiving plane is already represented in the coplanar irradiance measurement. This quantity is not direct-normal irradiance. The SP-212's spectral and angular responses differ from those of concentrating multi-junction optics [11]; its calibration and angular response, and the concentrator's limited collection of diffuse light, remain relevant to the uncertainty and interpretation. Offline scaling also does not retroactively correct firmware irradiance thresholds or change historical control decisions. No experiment-specific uncertainty budget is available for shunt resistance, amplifier gain, voltage reference or irradiance calibration. Reported decimal places identify reproducible calculations, not a demonstrated metrological precision or confidence interval.

Every observation retains its source line, raw codes and quality flags. Checks include signed conversion, channel clipping, a 99%-of-current-rail guard, negative channels, timestamps and uptime discontinuities. For integration, both adjacent endpoints must be electrically accepted and illuminated ($G > 50$ W m^{-2}), their separation must be positive and at most 15 s, and uptime must not decrease. Rejected observations and long gaps are never bridged. Low output and manual interventions are retained, not excluded because they reduce a performance score. Clock-hour subdivisions are descriptive and accompany, rather than replace, the complete acquired record.

3.3. Estimated output and aperture-referenced performance

The instantaneous available-MPP proxy and its energy integral are

$$\widehat{P}_{\mathrm{MPP}} = I_{sc} V_{oc} FF, \qquad \widehat{E} = \int_{\mathcal{S}} \widehat{P}_{\mathrm{MPP}}\, dt, \qquad FF = 0.82, \tag{2}$$

where $\mathcal{S}$ is the union of accepted adjacent intervals and time is expressed in hours for Wh. A fixed fill factor is assumed; no outdoor I–V curve, MPP converter or delivered-load power is inferred. Sequential sensing further assumes approximately stable conditions across the conversion cycle, which can fail during rapid changes. Thus $\widehat{E}$ estimates available electrical energy, not harvested or net system energy.

On the identical temporal support, define

$$H = \int_{\mathcal{S}} G\, dt, \qquad \widehat{\eta}_{\mathrm{ap},E} = \frac{\widehat{E}}{A_L H}, \qquad \widehat{\eta}_{\mathrm{ap}}(t) = \frac{\widehat{P}_{\mathrm{MPP}}(t)}{A_L G(t)}. \tag{3}$$

The integrated ratio, reported as a percentage, is not the mean of the instantaneous ratios. With the confirmed coplanar irradiance measurement, it estimates the complete lens/receiver combination's electrical conversion relative to solar energy incident on its aperture, not intrinsic cell efficiency. Optical losses that reduce the measured cell response are already reflected in the numerator; no additional lens-transmission factor is applied to that output. For any alternative constant FF', $\widehat{E}$ and $\widehat{\eta}_{\mathrm{ap},E}$ scale by $FF'/0.82$; this is sensitivity to an assumption, not a calibrated uncertainty interval.

3.4. Relative response without an ideal-alignment claim

To describe electrical response relative to a common empirical reference, let $R(t) = I_{sc}(t)/G(t)$ and consider both its full-record maximum $R_{\max}$ and 99th percentile R_{99}. For either reference R_*,

$$\widehat{P}_{\mathrm{ref}}(t; R_*) = R_* G(t) V_{oc}(t) FF, \qquad \rho_E(R_*) = \frac{\int_{\mathcal{S}} \widehat{P}_{\mathrm{MPP}} dt}{\int_{\mathcal{S}} \widehat{P}_{\mathrm{ref}}(t; R_*) dt}. \tag{4}$$

This is a record-specific relative-yield indicator, not independently validated tracking efficiency or angular accuracy. Neither reference removes temperature, spectral, geometry or asynchronous-sensing effects. The P99 reference is not a strict ceiling; ratios are not clipped to 100%. Sensitivity to reference choice is part of the result, not a reason to select the reference that produces the most favorable number.

3.5. Equal-area fixed-silicon reference scenario

No simultaneous silicon reference measurement accompanies the acquisition. We therefore define a conditional equal-area scenario for a hypothetical fixed silicon surface coplanar with the lens, using the measured plane-of-aperture irradiance and the accepted temporal support of the CPV estimate:

$$P_{\mathrm{Si,scenario}}(t) = A_L \eta_{\mathrm{Si}} G(t), \qquad E_{\mathrm{Si,scenario}} = A_L \eta_{\mathrm{Si}} H, \qquad B = \frac{\widehat{E}}{E_{\mathrm{Si,scenario}}}. \tag{5}$$

PVWatts lists approximate nominal module efficiencies of 19% and 21% for its Standard and Premium crystalline-silicon categories, respectively [12]. These two assumptions provide model-based context, not upper/lower bounds on silicon technology or specifications of a tested panel. The equivalent area is a normalization, not a fabricated 0.002497-m^2 module. This scenario does not assume equal rated power or equal cell area. Since $B = \widehat{\eta}_{\mathrm{ap},E}/\eta_{\mathrm{Si}}$ under these assumptions, the comparison is an algebraic restatement of the aperture estimate, not independent experimental evidence.

Holding silicon efficiency constant isolates the area/irradiation comparison; it does not predict temperature-corrected field yield. A physical module model would additionally require module-specific optical corrections to the measured plane irradiance, cell temperature and thermal mounting conditions [13, 14]. PVWatts' corresponding nominal power-temperature coefficients are −0.37 and −0.35%/K, but no unmeasured silicon temperature is assigned here. Coplanarity supports the common incident irradiance basis, but does not equate absorbed effective irradiance or measured electrical output for the two technologies. Values of B are conditional arithmetic comparisons, not measured energy gains over silicon.

4. Field Results

4.1. Acquisition coverage and operating chronology

The acquired span is 09:52:50–16:05:13, comprising 5,049 electrical/coordinate observations and 5,026 separate telemetry messages. All main observations pass the ADC quality checks and exceed the analysis illumination threshold. There are no duplicate main timestamps or decreasing main-sample uptimes. Five gaps exceed 15 s: 09:53:10–09:53:51 (41 s); 09:54:11–09:57:17 (186 s); 10:34:38–10:34:59 (21 s); 16:03:43–16:04:23 (40 s); 16:04:43–16:05:01 (18 s). Excluding these gaps gives 6.121 h of integration support out of 6.206 h elapsed, or 98.63% coverage. The audit retains every acquired observation; no clipped samples or unobserved intervals are reconstructed.

The complete overview in Fig. 2 connects electrical response with stage motion. There are 61 logged remote commands, including early tuning and repositioning. For example, `Delay=4` was logged at 12:27:20, before the 12:32 boundary. Three event boundaries divide the record without selecting a favorable performance threshold: `ErrMax=1100` at 12:32:02, `ErrMax=1000` at 13:53:00, and the first late manual-coordinate command at 15:12:42. All four sequential phases are retained in Table 2. No additional remote commands are recorded inside the 12:32–13:53 phase; periodic controller reference resets continue. This is an interval without logged operator interventions, not a controlled comparison of firmware or settings.

4.2. Electrical output and aperture estimate

Applying Eqs. (2)–(3) over the complete accepted support yields 3.746 Wh of estimated available-MPP energy from 6.408 kWh m^{-2} of measured aperture-plane irradiation, with an energy-weighted aperture estimate of 23.41%. Table 1 shows every acquired clock-hour bin, including the initial low response and late decline, rather than replacing the complete record with a midday-only integral.

At the maximum of the power estimate (2026-11-04 12:27:40), the sequentially recorded values in that observation were I_{sc} = 502.0 mA, V_{oc} = 2.361 V and G = 1172.1 W m^{-2}, giving 0.972 W estimated output and an instantaneous aperture estimate of 33.21% at that observation. Separate maxima are not combined into a synthetic operating point. The 12:32–13:53 phase

contributes 1.126 Wh over 1.349 h, with an aperture estimate of 28.47%. The 15:00–16:00 clock-hour estimate falls to 11.51%, and the phase after the first 15:12 manual command gives 6.97%. The record shows deterioration before and after that command, not evidence that the command alone caused it.

Table 1: Complete acquisition and fixed clock-hour summaries. H is aperture-plane irradiation, $\widehat{E}$ is FF-based available energy and $\widehat{\eta}_{\mathrm{ap},E}$ is the energy-weighted aperture estimate. Bins contain only acquired observations. Both edge endpoints must lie inside a bin, so subdivided integrals omit boundary-crossing edges and need not sum exactly to the full-record integral.

Window	N	Support [h]	H [kWh m^{-2}]	$\widehat{E}$ [Wh]	$\widehat{\eta}_{\mathrm{ap},E}$ [%]
Full acquired record	5049	6.121	6.408	3.7463	23.41
09:00–10:00	41	0.056	0.046	0.0002	0.21
10:00–11:00	717	0.993	0.945	0.4629	19.61
11:00–12:00	718	0.998	1.100	0.7387	26.90
12:00–13:00	807	1.000	1.173	0.8094	27.65
13:00–14:00	900	0.999	1.165	0.8004	27.51
14:00–15:00	900	0.999	1.104	0.6887	24.97
15:00–16:00	900	0.999	0.838	0.2409	11.51
16:00–17:00	66	0.070	0.029	0.0004	0.58

Table 2: All sequential event-defined phases. Internal command boundaries belong to the following phase; the final acquired sample is retained. As in Table 1, edges crossing a boundary are omitted. Phases describe operation; they are not matched experimental treatments.

Phase boundary clocks	N	Support [h]	$\widehat{E}$ [Wh]	$\widehat{\eta}_{\mathrm{ap},E}$ [%]
09:52:50–12:32:02	1863	2.584	1.601	23.61
12:32:02–13:53:00	1215	1.349	1.126	28.47
13:53:00–15:12:42	1195	1.327	0.903	24.95
15:12:42–16:05:13	776	0.859	0.114	6.97

4.3. Relative response and solar-position context

An empirical same-record I_{sc}/G reference is highly sensitive to one point: the maximum is 0.001078 A m^2 W^{-1} at 2026-11-04 13:01:07, where G = 313.0 W m^{-2} and I_{sc} = 337.2 mA; the P99 reference is 0.000420 A m^2 W^{-1}. The anomalous sample is retained. In its four-minute neighborhood, median irradiance is 1186.6 W m^{-2} (61 samples), consistent with an isolated irradiance dip rather than sustained low irradiance; the cause remains unresolved. Across the accepted illuminated samples, median I_{sc}/G is 0.000335 A m^2 W^{-1} (interquartile range 0.000250–0.000376). Full-record integrated relative-yield indicators are 28.9% (maximum reference) and 74.1% (P99 sensitivity). These are internal, reference-dependent indicators rather than independently validated tracking efficiencies. Figure 4 displays both the full responsivity range and a typical-range view; the anomalous observation remains in the analysis.

Interpolated SunCalc positions at the first and last observations are 130.25° and 238.89° azimuth, with elevations 35.86° and 25.89°, respectively. The printed table reaches 52.59° elevation at 12:30. Figure 3 relates this trajectory to the measured normalized response. Logged

coordinates span $X = 0$–$114,000$ and $Y = 1,800$–$104,965$ steps. These are observed solar and coordinate ranges, not independently validated acceptance angles or rated mechanical limits.

4.4. Conditional fixed-silicon reference

The coplanar, equal-area scenarios of Eq. (5) yield 3.040 and 3.360 Wh, respectively; the corresponding estimated-CPV-to-scenario ratios are 1.232 and 1.115. Figure 5 illustrates these assumptions, not measured comparative yields. Changing the assumed CPV fill factor from 0.82 to 0.70 or 0.90 would change the full-record energy estimate to 3.198 or 4.112 Wh, respectively. This sensitivity range is illustrative, not a measured uncertainty interval.

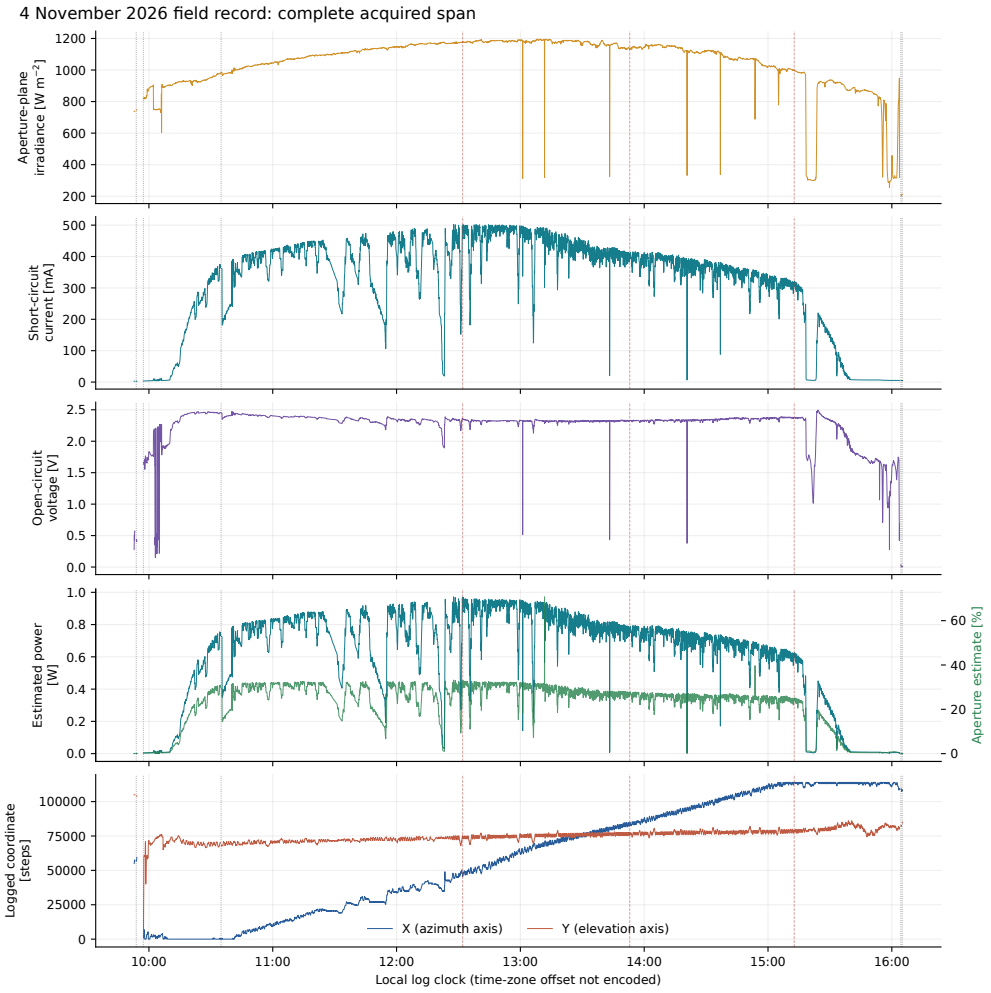


Figure 2: Complete 4 November acquisition. Vertical dotted lines mark sampling gaps; dashed lines mark the three selected phase-boundary commands. Raw trends are not smoothed, and gaps are not bridged. Electrical output is estimated using $FF = 0.82$.

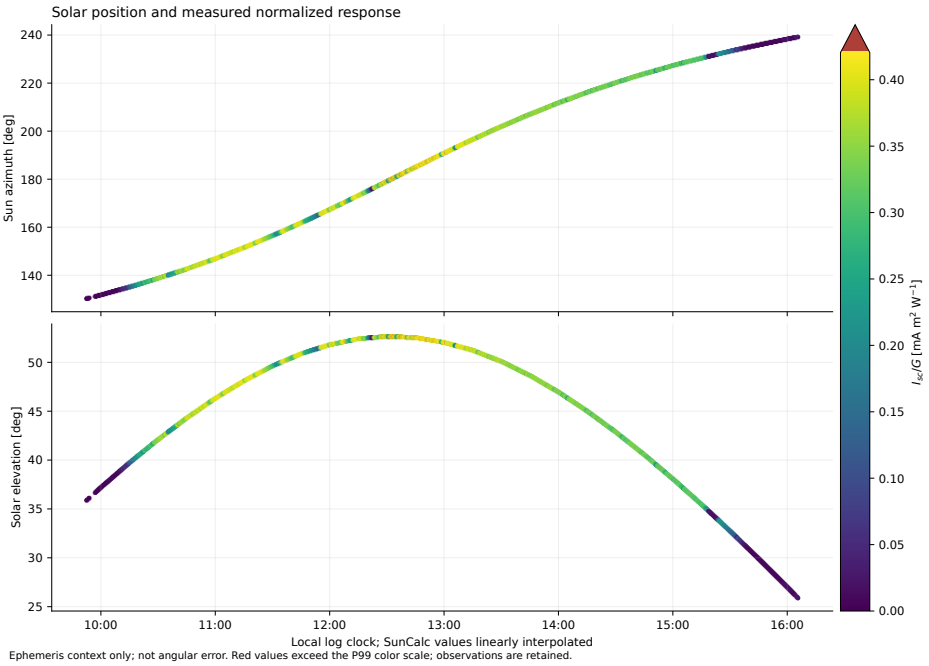


Figure 3: SunCalc azimuth/elevation context aligned to the measured response. SunCalc entries are spaced 15 minutes; intermediate positions are linearly interpolated for plotting. Color encodes I_{sc}/G, not pointing error; values above P99 remain plotted in the red over-range color.

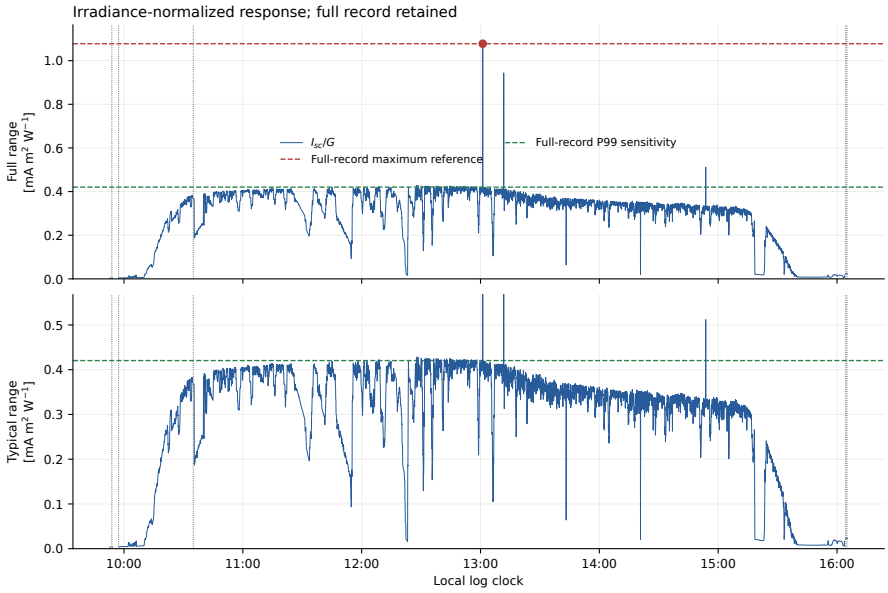


Figure 4: Irradiance-normalized response for the full record. The maximum reference is dominated by a retained anomalous observation; P99 is shown only as a sensitivity analysis. Neither line is an independent ideal-tracking standard.

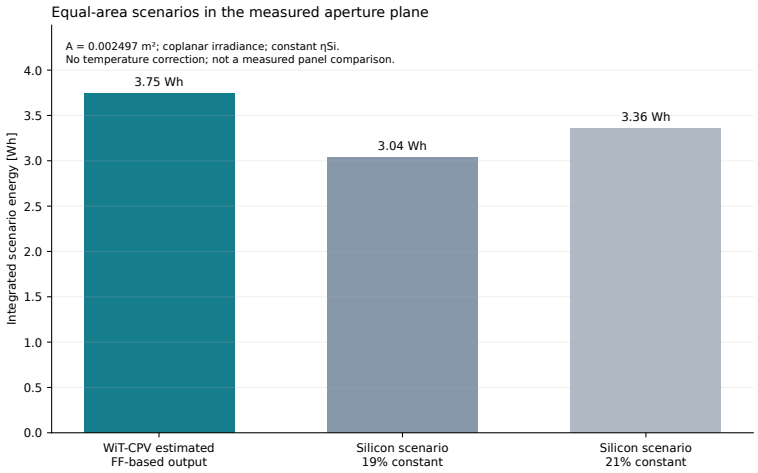


Figure 5: Conditional equal-area scenarios using the measured aperture-plane irradiance. Silicon efficiency is held constant at 19% or 21%; no panel, temperature correction or measured head-to-head comparison is represented.

5. Discussion

5.1. What the principal experiment establishes

The principal result is a single, traceable operating characterization that connects internal motion, electrical response and solar-position context. The unsaturated current channel permits analysis of the acquired daytime span without reconstructing clipped high-current observations. The 23.41% integrated aperture estimate retains initialization, tuning and degraded response; it is therefore more informative about this record than a favorable midday peak alone. The useful output during changing solar direction supports the feasibility of internal receiver tracking, but does not isolate the controller's contribution from manual intervention or establish an ideal focal trajectory.

The lower late response is part of the demonstrated behavior, not a discarded outlier. Finite travel, optical acceptance, alignment, temperature and control settings could all contribute. Solar ephemerides and commanded coordinates alone cannot separate them. Establishing an angular operating envelope requires known external-optics orientation and an independent mapping between receiver position, incidence angle and optical response.

5.2. Why relative tracking and aperture efficiency differ

The aperture metric compares estimated electrical output with measured reference irradiation; the relative-yield metric instead compares against a same-record electrical responsivity. They answer different questions. An anomalously low irradiance reading can inflate both instantaneous aperture efficiency and a maximum-responsivity reference while depressing the maximum-referenced full-record ratio. A stable-looking current trace does not resolve whether a brief discrepancy arose from weather, sensor shading, electrical acquisition or different sensor/device response.

Consequently, the reference sensitivity must not be compressed into one unqualified tracking-efficiency headline. Even a robust percentile reference remains empirical, reuses the measured

voltage and cannot independently measure perfect alignment. Irradiance normalization also cannot distinguish thermal drift from small alignment-induced changes. The record does not validate cloud-recovery time or the causal benefit of a specific protective branch; those require controlled perturbations or independently characterized disturbances.

5.3. Interpreting the silicon comparison and next validation

The shared-reference scenario places the aperture estimate alongside transparent nominal silicon-efficiency assumptions, without treating the CPV aperture as externally tracked at normal incidence. Its dependencies are the assumed fill factor and silicon efficiency, together with unmeasured temperature and module-specific optical response. The confirmed coplanar sensor provides the incident-irradiance basis for the equal-plane scenario. Different diffuse, spectral and angular responses prevent extrapolating the scenario to annual yield or arbitrary weather. No economic or lifecycle advantage is inferred.

A simultaneous experiment should measure silicon DC output at MPP, document module area and datasheet parameters, and record tilt, azimuth, coplanar irradiance and module temperature. Equivalent delivered-energy claims also require CPV operation into a measured load rather than alternating I_{sc}/V_{oc} sensing. For net energy, the complete board and motor supply must be logged. Fine-tuning counters omit other moves, and sampled coordinate differences can miss reversals; neither substitutes for supply-energy measurement. The most useful next campaign therefore combines those measurements with fixed documented settings and repeated days, followed by controlled controller-version comparisons.

6. Conclusions

The 4 November 2026 acquisition provides a coherent principal field case for the tracking-integrated WiT-CPV prototype: 5,049 observations, 6.121 h of accepted integration support, and no ADC clipping. With a nominal 0.130-Ω shunt, corrected pyranometer scaling and an assumed $FF = 0.82$, the available-MPP energy estimate is 3.746 Wh for 6.408 $\mathrm{kWh\,m^{-2}}$ of reference irradiation. The resulting energy-weighted, aperture-referenced estimate is 23.41%. These quantities characterize the lens/receiver system against the recorded irradiance, rather than intrinsic cell efficiency or measured harvested energy.

Linking the response to the solar-position reference and stage trajectory reveals useful operation as well as late degradation. The event-defined 12:32–13:53 phase has no additional logged remote commands and yields an aperture estimate of 28.47%, providing a post-tuning operating case alongside the complete-record result. Retaining tuning commands and low-output periods makes the result a characterization of observed operation, not a claim of autonomous full-day lock. A pronounced irradiance anomaly also demonstrates why a same-record maximum cannot be treated as an independently validated ideal-tracking reference.

Under the shared-pyranometer, constant-efficiency assumptions, the estimated CPV energy corresponds to ratios of 1.232 and 1.115 relative to the 19% and 21% equal-area silicon scenarios. These are arithmetic scenario ratios, not measured comparative yields or evidence of superiority over a fixed panel. The decisive next validation is simultaneous delivered-MPP and parasitic-power measurement, with matched receiving planes, measured temperature and fixed control settings. This would turn the present aperture-level characterization into a test of repeatable net system benefit.

Reproducibility

The companion analysis retains the raw observations, source-line references, quality flags, accepted integration edges and command chronology. Its machine-readable summary records source hashes and assumptions; the supplied SunCalc table is transcribed separately. Numerical tests cover calibration, gap handling, integration and scenario scaling. All result tables and field figures are regenerated from these inputs, without modifying the raw log.

References

[1] Hossein Mousazadeh et al. "A review of principle and sun-tracking methods for maximizing solar systems output". In: *Renewable and sustainable energy reviews* 13.8 (2009), pp. 1800–1818. DOI: 10.1016/j.rser.2009.01.022.

[2] AZ Hafez, AM Yousef, and NM Harag. "Solar tracking systems: Technologies and trackers drive types–A review". In: *Renewable and Sustainable Energy Reviews* 91 (2018), pp. 754–782. DOI: 10.1016/j.rser.2018.03.094.

[3] Rosa F Fuentes-Morales et al. "Control algorithms applied to active solar tracking systems: A review". In: *Solar Energy* 212 (2020), pp. 203–219. DOI: 10.1016/j.solener.2020.10.071.

[4] Waseem Iqbal, Irfan Ullah, and Seoyong Shin. "Optical developments in concentrator photovoltaic systems—a review". In: *Sustainability* 15.13 (2023), p. 10554. DOI: 10.3390/su151310554.

[5] Maria A Ceballos et al. "Tracking-Integrated CPV Technology: State-of-the-Art and Classification". In: *Energies* 16.15 (2023), p. 5605. DOI: 10.3390/en16155605.

[6] Atsushi Ito, Daisuke Sato, and Noboru Yamada. "Optical design and demonstration of microtracking CPV module with bi-convex aspheric lens array". In: *Optics Express* 26.18 (2018), A879–A891. DOI: 10.1364/OE.26.00A879.

[7] S. Askins et al. "Performance of hybrid micro-concentrator module with integrated planar tracking and diffuse light collection". In: *2019 IEEE 46th Photovoltaic Specialists Conference (PVSC)*. IEEE. 2019, pp. 2507–2512. DOI: 10.1109/PVSC40753.2019.8980519.

[8] Kareem Younes et al. "Realizing high photovoltaic power densities with tracking-integrated concentrator photovoltaics". In: *Frontiers in Energy Research* 10 (2022), p. 842201. DOI: 10.3389/fenrg.2022.842201.

[9] Arturo Díaz-Ponce et al. "Development of a proof-of-concept concentrating photovoltaic module with integrated tracking and azimuthal cell rotation". In: *Results in Engineering* 27 (2025), p. 106735. DOI: 10.1016/j.rineng.2025.106735.

[10] Torsten Hoffmann. *SunCalc: Daily Solar-Position Data for Aguascalientes, 4 November 2026*. Supplied printout at latitude 21.87304 degrees N and longitude 102.28282 degrees W; local-time azimuth and elevation at 15-minute intervals. 2026. URL: https://www.suncalc.org/ (visited on 11/04/2026).

[11] Apogee Instruments. *SP-212/SP-215 Pyranometer Instruction Manual*. URL: https://www.apogeeinstruments.com/content/SP-212-215-manual.pdf (visited on 11/04/2026).

[12] PVWatts. *Module Type*. Standard and Premium crystalline-silicon module assumptions. URL: https://pvwatts.nlr.gov/docs/help_module_type.php (visited on 11/04/2026).

[13] Sandia National Laboratories. *Plane of Array (POA) Irradiance*. PV Performance Modeling Collaborative. URL: https://pvpmc.sandia.gov/modeling-guide/1-weather-design-inputs/plane-of-array-poa-irradiance/ (visited on 11/04/2026).

[14] Sandia National Laboratories. *PVWatts*. PV Performance Modeling Collaborative. URL: https://pvpmc.sandia.gov/modeling-guide/2-dc-module-iv/point-value-models/pvwatts/ (visited on 11/04/2026).